

Scaling of surface roughness and polymer structure in a model for film growth and polymerization

Jônatas A. R. Euzébio^{1,*} and F. D. A. Aarão Reis^{1,2,†}¹*Instituto de Física, Universidade Federal Fluminense, Avenida Litorânea s/n, Niterói 24210-340, RJ, Brazil*²*Department of Chemistry, University of Wisconsin–Madison, Madison, Wisconsin 53705, USA*

(Received 12 April 2009; revised manuscript received 16 June 2009; published 19 August 2009)

We study a model of growth of polymer films using numerical simulations and scaling concepts. During the deposition, each new monomer flows in a direction perpendicular to the substrate, aggregates at the first contact with the deposit and executes up to G steps along the polymers, propagating an existing chain or nucleating of a new polymer. Some qualitative results agree with those of a previous model for vapor deposition polymerization (VDP) with collective diffusion, such as the roughness increase and density decrease with G . This supports the interpretation of G as a ratio between diffusion coefficient and monomer flux. We perform a systematic study of scaling properties of the outer surface roughness and of polymer size and shape. For large G , the polymers are stretched in the direction perpendicular to the substrate and have typical size increasing as $G^{1/2}$. This is explained by the solution of the problem of random walk trapping, which illustrates the connection of surface processes and bulk properties. The distributions of polymer sizes are monotonically decreasing for all G and very broad, thus a large number of small chains and of chains much larger than the average is found in typical samples. The outer surface roughness obeys Kardar-Parisi-Zhang scaling, in contrast to the apparent anomalous scaling of previous VDP models with oblique monomer flux. However, the calculation of reliable exponents requires accounting for huge finite-size corrections. Possible applications and extensions of this model are discussed.

DOI: [10.1103/PhysRevE.80.021605](https://doi.org/10.1103/PhysRevE.80.021605)

PACS number(s): 81.15.Aa, 68.47.Mn, 68.35.Ct, 68.55.J–

I. INTRODUCTION

Chemical vapor deposition polymerization (CVDP) and variants of this technique have attracted increasing interest in the last years and were used to produce nanostructures of several materials [1–13]. The basic steps of CVDP are the sublimation of one or more polymers (or oligomers), their pyrolysis in a region of much higher temperature and the deposition of the resulting monomers on a substrate where polymerization occurs. An advantage of this process over the preparation methods in solution is to require no catalyst, solvent, or initiator, thus avoiding the presence of undesired materials in the final sample. Such features can be extremely important for biomedical applications [14,15].

Some models were already proposed to describe CVDP kinetics and film properties. Kinetic models based on rate equations can explain the main effects of temperature and pressure on growth rates without describing the film structure [16,17]. On the other hand, to our knowledge only one type of model was proposed to represent the polymer structure in those films [18–20]. It included diffusion of physisorbed monomers, but polymers were rigid due to computational restrictions to simulate polymer dynamics in large samples. This approach resembles the modeling of metal and semiconductor deposition, where the competition between deposition and diffusion determines the scaling properties of the film [21]. Previous work on that model discussed the qualitative effects of monomer diffusion on density and polymer size, showed the stretching of long polymers, and proposed that surface roughness scaling is anomalous [19,20].

However, some important questions were not fully addressed yet, or deserve a deeper investigation. One example is the relation between the conformational properties of the polymers and the ratio $G \equiv D/F$ between diffusion coefficient (D) and deposition flux (F). The scaling of polymer size distribution, the statistics of closed and open chains, and the roughness of the outer surface are other relevant properties for many applications.

The aim of the present work is to address these questions in a model of growth and polymerization. The monomer dynamics at the deposit parallels that of the model introduced by Bowie and Zhao [19], but with a limited mobility condition, and the monomer flux is perpendicular to the substrate. Among the results presented here, we show that the average polymer size scales as $G^{1/2}$, and explain this result through the relation with the random walk trapping problem. This emphasizes the idea of obtaining bulk properties by connections with surface processes [22,23]. However, there are significant corrections to scaling even in data obtained in very large samples. If one does not account for those corrections, they may lead to wrong interpretation of a relatively simple and universal system dynamics. This is also important in the study of the outer surface: we will show evidence that the roughness obeys Kardar-Parisi-Zhang (KPZ) [24] scaling, with deviations in exponent estimates similar to those found in other models and real systems [23,25,26]. This finding contrasts to the proposal of anomalous scaling of Ref. [20] for the CVDP model with oblique (cosine) flux of monomers. Our simulations are performed in two dimensions, but our scaling approach can be extended to three-dimensional systems, which enables the discussion of possible applications.

The rest of this paper is organized as follows. In Sec. II, we will present our model and justify its assumptions. In Sec. III, we will discuss properties that can be compared with

*jonatas@if.uff.br

†Corresponding author; reis@if.uff.br

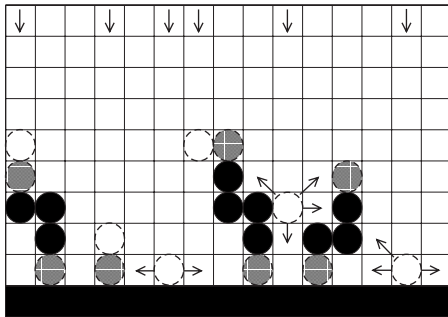


FIG. 1. Scheme of the deposition, diffusion, and aggregation rules. The deposited polymers contain intermediate monomers (in black) and end monomers (in gray). Columns of incidence of new monomers are indicated by vertical arrows at the top, and the positions where they aggregate to the deposit are indicated by open circles with dashed boundary. The possible movements of those monomers immediately after aggregation are indicated by arrows (monomers aggregating at chain ends do not move anymore).

previous related models: film density and shape-size relation of the polymers. In Sec. IV, we will study the scaling of the surface roughness, with a focus on universal features and scaling corrections. In Sec. V, we will study the polymer morphology. In Sec. VI we summarize our results and present our conclusions.

II. MODEL FOR POLYMERIZATION AND FILM GROWTH

Our model is illustrated in Fig. 1 in a square lattice (xz plane), where we performed the simulations (extension to a cubic lattice is straightforward). The substrate occupies the line $z=0$ and each site with $z>0$ may be empty or occupied by a monomer. The monomer size sets the relevant length scales of this system, thus each site has 0.5–2 nm of size for most applications. Only the formation of linear polymers is allowed. The growth (propagation) of a deposited polymer occurs by attachment of a new monomer to one of its ends, which are called active tips.

The growth dynamics proceeds as follows. At each time step, a new monomer is released from a randomly chosen position far above the film surface, follows a trajectory perpendicular to the substrate and stops upon first contact with a nearest-neighbor occupied site. If that position has a nearest-neighbor active tip, then the monomer aggregates permanently there, propagating that chain. Otherwise, that monomer executes a maximum of G random steps to nearest neighbor or next-nearest-neighbor sites, with equal probabilities (the limitation in the number of steps relates deposition and diffusion rates, as will be explained below). The step trial is accepted only if the target site has at least one occupied nearest neighbor, which may be a polymer or the substrate. During its diffusion, if this monomer encounters a polymer end or another monomer in a nearest neighbor site, it permanently aggregates at that position. If the monomer does not find an active tip after G steps, it permanently aggregates at its final position and becomes the active tip of a new polymer (this corresponds to nucleation of a new polymer).

When the diffusing monomer encounters only one active tip at a neighboring site, it becomes the new active tip of the polymer. If the monomer simultaneously encounters two active tips of the same polymer, that chain is closed. If the two neighboring active tips belong to different polymers, they coalesce, i.e., they become a single longer chain. Finally, if the monomer encounters three active tips, it reacts with two of them, forming a longer chain or a closed polymer. All processes in which a diffusing monomer encounters two or more active tips are rare, mainly for large G .

Our model is of limited mobility because the diffusion of only one monomer is simulated at each time. However, we can set a correspondence between our model parameters and processes with collective diffusion, with a flux of F particles (atoms, molecules etc.) per column per unit time and D surface steps of each particle per unit time. In a compact film, the average number of steps a particle executes before being buried by another particle is

$$G \equiv D/F. \quad (1)$$

For a porous film with density not too low, which is the case in our model, the order of magnitude of G is still given by Eq. (1).

Our approach resembles the limited mobility models for molecular beam epitaxy (MBE) [27,28], in contrast to full (or collective) diffusion models [21], where simultaneous diffusion of many atoms or molecules is simulated. The CVDP model of Ref. [19] is also an example with full diffusion. One possible concern about the limited mobility assumption is the possibility of finding many isolated monomers in energetically unfavorable positions after their G steps, which is less probable in full diffusion models. However, our simulations show that nearly 2% of the deposited monomers is isolated in films grown with $G=10$, and much smaller fractions for large G (a discussion of the polymer size distributions is provided in Sec. V). Thus, the effects of these isolated monomers are negligible, and our model actually leads to significant polymerization, although many incident monomers stop moving without forming a permanent bond immediately after their G steps.

Previous works on CVDP models [19,20] also simulated monomer fluxes obeying a cosine law, while here we consider a vertical flux. However, the surface roughness and film density have the same order of magnitude of our model for the same G , probably because small angles dominate the cosine flux (significant changes would be expected, for instance, in cases of completely oblique flux [3]).

On the other hand, a common feature of our model and previous ones is to neglect chain relaxation, which allows simulation of large deposits with many polymers. Chain relaxation is expected in real CVDP, even for rapid deposition, but our assumption is an interesting starting point for studying the role of monomer surface diffusion independently of other processes. Other assumptions common to our model and previous ones are the large rates of polymer initiation and propagation reactions, when compared to deposition and diffusion rates, and absence of desorption.

Our simulations were performed in lattices of lengths $L=16$ to $L=128$ until the regime of roughness saturation

(steady state of dynamic scaling). The model was also simulated in lattices of length $L=1024$ during the roughness growth regime, with deposition of nearly 10^4 monomers per site. The time unit is defined as the time necessary for deposition of one layer of monomers, i. e. it corresponds to a time $1/F$. Diffusion to deposition ratios varying from $G=10$ to $G=10^4$ was studied. The number of realizations for each G and lattice size varied from 100 to 1000. A sequence of monomer positions of each growing polymer was stored during the simulation and used to calculate average quantities. Some averages were also calculated only for polymers above a certain distance from the substrate (varying from 20 to 700), but no significant difference was found. This suggests that flat substrate effects are weak.

In porous deposits, such as those produced by CVDP models, many atoms or molecules at the same column are in contact with the external media. Thus the interface between the solid and the gas phases is multivalued. However, it is important to characterize the outer surface of the deposit, which is accessible through surface imaging methods. In this surface, the height h of each column is that of the highest particle (atom, monomer etc) at that column. Thus, the roughness W is defined as

$$W(L,t) \equiv [\langle (h - \bar{h})^2 \rangle]^{1/2}, \quad (2)$$

where the overbars indicate spatial averages and the angular brackets indicate configurational averages.

Another interesting quantity to characterize surface features is the height-height correlation function

$$C(r,t) \equiv \langle h(r_0,t)h(r_0+r,t) \rangle \quad (3)$$

at distance r and time t , with h measured relatively to the average film height and averages over different initial positions r_0 and different configurations.

III. COMPARISON WITH PREVIOUS RESULTS ON CVDP MODELING

In Figs. 2(a) and 2(b), we show regions of deposits grown with $G=10$ and $G=10^4$, and highlight some of their polymers. Two features are clearly similar to the full diffusion models [19,20]: as G increases, the film becomes less compact and the polymers are longer and stretched in the vertical direction. However, the main difference is that the cosine flux produces treelike structures in the deposit, with some polymers growing along oblique directions. That flux produces larger surface mounds and decreases the film density, mainly for large G (see Ref. [20]), while the vertical flux allows monomers to penetrate deeper below the external surface, increasing the density. We believe that this difference does not change qualitative trends because the cosine flux is dominated by low angles and monomer diffusion reduces the shadowing effects.

In Fig. 3(a) we show the surface roughness of the deposits as a function of time, for several values of G . Similarly to Refs. [19,20], the roughness increases as G increases. The images in Figs. 2(a) and 2(b) (and also Fig. 4 of Ref. [20]) help to explain this result: as G increases, the depth of the

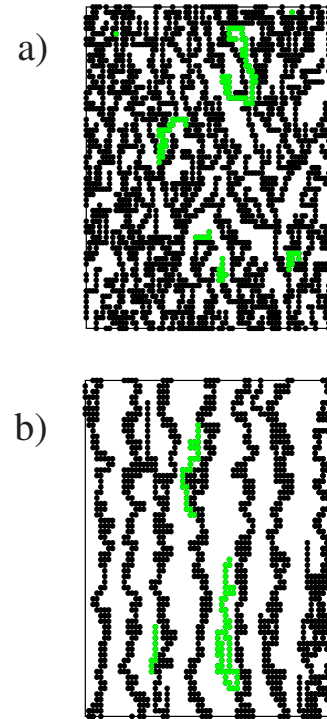


FIG. 2. (Color online) Sections with lateral size of 64 lattice units of deposits grown with (a) $G=10$ and (b) $G=10^4$.

valleys separating the long polymers in the surface increase. It contrasts to the decrease of roughness in MBE growth as the temperature increases. Indeed, while larger temperature favors atoms to form more compact structures in MBE growth, it favors the formation of longer polymers in the CVDP model, with larger free space between them. A deeper analysis of dynamic scaling of surface roughness in our model is presented in Sec. IV.

There are experimental works on CVDP showing roughness increase with the substrate temperature, such as deposition of poly(p-xylylene) films of Ref. [9]. However, the opposite occurred in growth of poly(cyano-p-xylylene) films by Buzin *et al.* [10]. Possibly the latter result is a consequence of significant chain relaxation compared to the former. There are also experiments only with polymer sublimation and condensation (i.e., without polymerization) which show roughness increasing with temperature [29,30]. Recent works also analyzed the effect of decomposition (pyrolysis) temperature on film roughness, and different trends were found; for instance, as that temperature increases, Ref. [11] reports increase of film roughness and Ref. [5] reports a decrease.

In Fig. 3(b), we show the film density ρ as a function of time. At long times, ρ slowly varies, particularly for large G . Extrapolation to $t \rightarrow \infty$ (typically assuming corrections in $1/t$ or $1/t^{1/2}$) gives $0.35 \leq \rho \leq 0.47$. The decrease of the density with increasing G agrees with the model of full diffusion [19]. A model of convective-diffusive particle deposition also shows vanishing density as a diffusion coefficient diverges [31]. However, it is important to note that the density change is very slow in the range of G analyzed here (approximately 25% for three orders of magnitude of change in G). Due to the deeper penetration of incident monomers, the density in

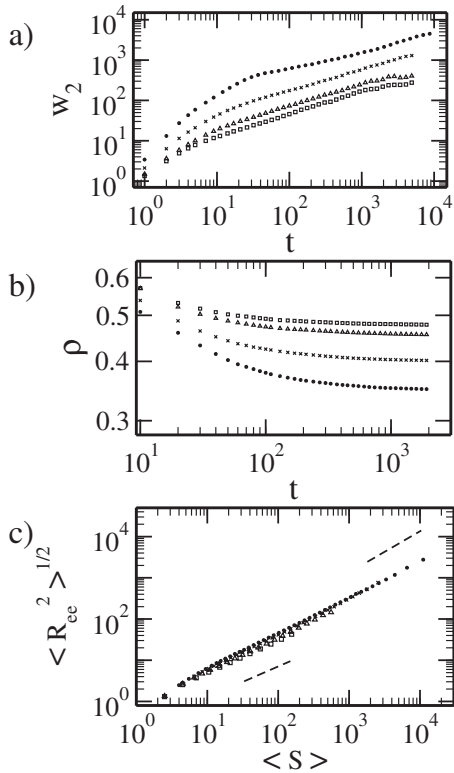


FIG. 3. (a) Surface roughness as a function of time. (b) Film density as a function of time. (c) Rms end-to-end distance of deposited chains as a function of chain size. Simulation data are for $G=10$ (squares), $G=10^2$ (triangles), $G=10^3$ (crosses), and $G=10^4$ (circles), in a lattice size $L=1024$. In (c), the dashed line at the bottom has slope $3/4$ and the one at the top has slope 1 .

our model is slightly smaller than that of Ref. [20] for the same G . On the other hand, Bowie and Zhao [19] show much larger densities, ranging approximately from 0.45 to 0.65 for $10 \leq G \leq 10^4$. Unfortunately, here we are not able to provide an explanation for this discrepancy.

Figure 3(c) shows the root mean square (rms) end-to-end distance $\langle R_{ee}^2 \rangle^{1/2}$ as a function of polymer size $\langle S \rangle$ (measured as the number of monomers in the chain). This plot shows a crossover from a slope near $3/4$ for small sizes to a slope near 1 for large sizes. The former is typical of self-avoiding walks (SAW) in two dimensions [32], while the latter characterizes polymers stretched in one direction. Inspection of Figs. 2(a) and 2(b) suggests that the polymers are elongated in the vertical direction. These results are also consistent with the findings of Refs. [19,20]. A deeper analysis of polymer morphology in our model is presented in Sec. V.

IV. DYNAMIC SCALING OF THE OUTER SURFACE ROUGHNESS

For $G=0$, our model is equivalent to the ballistic deposition (BD) model [33], in which incident particles permanently aggregate upon first contact with the deposit. The lateral aggregation of BD increases the column height of an amount proportional to the local height gradient. Simultaneously, it smoothes the surface by reducing the difference of

height from a nearest-neighbor column. These mechanisms are, respectively, expected to generate the nonlinear and the linear second order terms in a stochastic growth equation associated to BD (see e. g. Refs. [34,35]). That equation is the one of Kardar, Parisi, and Zhang, thus the roughness of ballistic deposits obeys KPZ scaling [24].

For $G > 0$, our model differs from BD due to the diffusion of aggregated monomers. The final position of these monomers are frequently far above the top particle at the same column, which is also expected to generate the KPZ nonlinearity. However, a numerical investigation of this claim is necessary, since diffusion favors final aggregation at active tips, which may lead to different growth velocities in hills and valleys (similarly to columnar growth). Moreover, a recent work on deposition of large particles and formation of porous deposits clearly shows a correspondence to a fourth order growth equation, which means cancellation of the KPZ nonlinearity [36].

In large substrates and not too long times, the surface roughness is expected to scale as

$$W \sim t^\beta, \tag{4}$$

where β is called the growth exponent. However, Fig. 3(a) shows that the roughness does not evolve as a simple power law: for small G , the slope of the $\log W \times \log t$ plot tend to decrease in time; for large G , it decreases for short times and increases after $t \sim 10^3$. Linear fits of the data in Fig. 3(a) for $t > 10^2$ give β between 0.27 and 0.28 for all G . (However, this fit does not account for the time evolution of the slopes of those plots.)

These estimates of β are well below the KPZ value $\beta = 1/3$, but they are very close to the BD values for the same lattice size $L=1024$ (see Ref. [37]). Consequently, that discrepancy cannot be related to a failure of asymptotic KPZ scaling. Instead, systematic data extrapolations to $L \rightarrow \infty$ are necessary to obtain reliable scaling exponents, similarly to previous work on BD [37–39]. Due to the difficulties to estimate β , we turn to the calculation of roughness and dynamic exponents.

In the regime of roughness saturation (very long times in a finite substrate), we expect the roughness to scale as

$$W_{sat} \sim L^\alpha, \tag{5}$$

where α is called the roughness exponent. In order to estimate α from W_{sat} , we extrapolate effective exponents defined as

$$\alpha_W(L) \equiv \frac{\ln[W_{sat}(L)/W_{sat}(L/2)]}{\ln 2}. \tag{6}$$

Figure 4(a) shows $\alpha_W(L)$ versus $1/L^{1/2}$ (the variable in the abscissa is the same that provides the best fits of BD data [37]). The parabolic fits shown in Fig. 4 extrapolate to $0.47 \leq \alpha \leq 0.53$ for all G . Those values are very close to the KPZ value $\alpha = 1/2$.

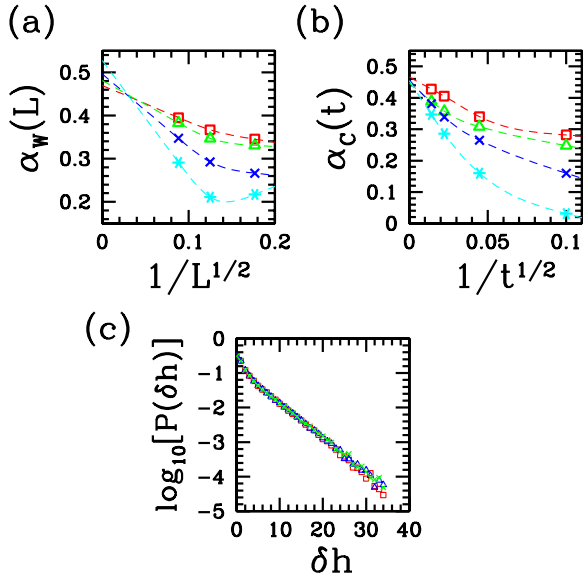


FIG. 4. (Color online) (a) Effective roughness exponent of the global roughness versus $1/L^{1/2}$. Dashed lines are parabolic fits of the data for each G . (b) Effective roughness exponent of the height-height correlation function versus $1/t^{1/2}$. Dashed lines are polynomial fits of the data for each G . Data in (a) and (b) are for $G=10$ (squares), $G=10^2$ (triangles), $G=10^3$ (crosses), and $G=10^4$ (asterisks). (c) Probability of nearest-neighbor step as a function of the step δh for $G=100$ at $t=100$ (red squares), $t=500$ (blue triangles), and $t=5000$ (green crosses).

Reference [20] reports anomalous scaling in the CVDP model with full diffusion and cosine flux. In such case, the global roughness exponent in Eq. (5) differs from the local roughness exponent in the scaling of the height-height correlation function [Eq. (3)],

$$C(r,t) \sim r^{2\alpha}. \quad (7)$$

We calculated $C(r,t)$ in the growth regime of large deposits ($L=1024$) for different times, between $t=100$ and $t=5000$. For each time, a scaling region is found, but the slope of that region is slightly different for different times (it always increases in time). Thus we calculated finite-time estimates of the (local) roughness exponent, $\alpha_C(t)$, defined analogously to Eq. (6). The procedure to find the best scaling region and the corresponding exponent followed the same lines of Ref. [40], where the local roughness was analyzed. Figure 4(b) shows $\alpha_C(t)$ versus $1/t^{1/2}$ for four values of G . Fits of the data for each G give asymptotic estimates ($t \rightarrow \infty$) between 0.45 and 0.47. They are very close to the exponents obtained from the global roughness W , in contrast to the anomalous scaling suggested in Ref. [20].

Another useful quantity to distinguish normal from anomalous scaling is the step distribution $P(\delta h)$, where $\delta h \equiv |h(x+1) - h(x)|$ is the difference in the heights of nearest neighbors [41]. This distribution is shown in Fig. 4(c) for $G=100$ in three different times, but results for the other values of G are similar. Two features reinforce the claim of normal scaling: the exponential decrease and, for fixed h , the constant value of $P(\delta h)$ as time increases.

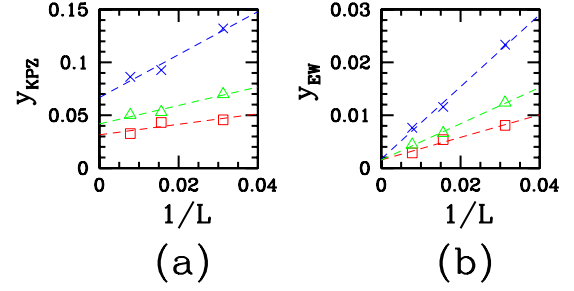


FIG. 5. (Color online) The ratios (a) y_{KPZ} and (b) y_{EW} versus $1/L$. The symbols correspond to the same values of G of Fig. 4 (shown data only up to $G=10^3$). Dashed lines are linear fits of the data for each G .

In two-dimensional deposits, the exponent $\alpha=1/2$ is the same for KPZ and for the linear second-order growth equation of Edwards and Wilkinson (EW) [42]. Thus we need further information to discard one of these two possibilities. We focus on the dynamic exponent z , which characterizes the scaling of the time t_\times of crossover to roughness saturation,

$$t_\times \sim L^z. \quad (8)$$

For EW growth, we have $z=2$, and for KPZ growth we have $z=3/2$.

We estimated t_\times following the procedure of Ref. [43]. In Figs. 5(a) and 5(b) we plot the reduced variables $y_{KPZ} \equiv t_\times/L^{3/2}$ and $y_{EW} \equiv t_\times/L^2$, respectively, as a function of $1/L$. As $L \rightarrow \infty$ ($1/L \rightarrow 0$), we observe that y_{KPZ} extrapolates to finite, nonzero and G -dependent values. On the other hand, y_{EW} rapidly decreases to values near zero for all G . This indicates KPZ scaling and discards EW.

We also measured roughness distributions [44,45] in the steady states of our model, since their comparison with other growth models have proved to be very useful for identifying universality classes (see, e.g., Ref. [23]). However, significant finite-size effects are also found for $L \geq 128$, and the steady state distributions of EW and KPZ classes are the same in 1+1 dimensions [44]. For these reasons, they do not improve the conclusions obtained from the roughness exponents.

As far as we know, dynamic scaling in CVDP was experimentally studied only in the poly(chloro-p-xylylene) films of Ref. [12]. An unusually large exponent $\beta \approx 0.65$ was obtained at short times, followed by crossovers to $\beta \approx 0$ for intermediate times and $\beta \approx 0.18$ for long times. The same work obtained α near or above 1. Comparison with our estimates is not possible because the exponents depend on the spatial dimension. However, the behavior of β and α in those experiments is similar to models of films with grainy structures at the surface [26]. Those models do have KPZ scaling, although exponent estimates show deviations from KPZ values [26]. Grainy structures at the surface of poly(isobenzofuran) films were also shown in Ref. [5]. Consequently, we believe that asymptotic KPZ scaling cannot be excluded in these systems. It is also interesting to mention that thin oligomer films with KPZ scaling were presented in Ref. [30]

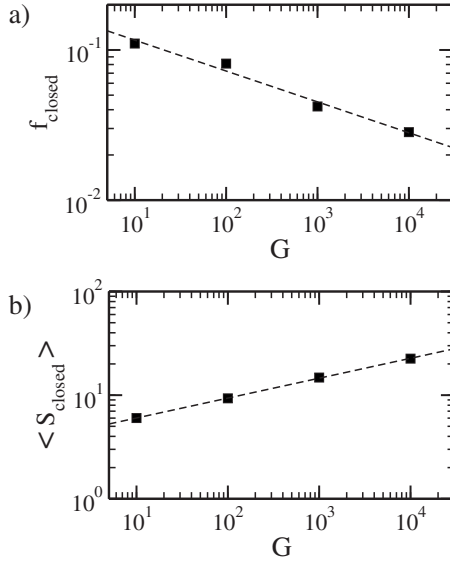


FIG. 6. (a) Fraction of closed polymers and (b) average size of closed polymers as a function of G . Data is from lattice size $L = 1024$. Dashed lines are linear fits of the data.

(in that case the molecule deposited as a whole in the substrate).

As shown in Fig. 4(c), the step size distributions of our model are significantly different from those of the CVDP model with cosine flux, which present power-law decays [20]. These distributions show small corrections to scaling, which means that they reliably describe the long time features of the model. This reinforces the conclusion on anomalous scaling in the model with cosine flux, thus belonging to a universality class different from our model.

V. EFFECTS OF DIFFUSION ON POLYMER PROPERTIES

First we analyze the role of closed polymers. In Figs. 6(a) and 6(b), we show their fraction f_{closed} and their average size $\langle S \rangle_{closed}$ as a function of G , respectively. Approximate scaling laws

$$f_{closed} \sim G^{-0.2} \quad (9)$$

and

$$\langle S_{closed} \rangle \sim G^{0.2} \quad (10)$$

are obtained in this range of G . The scaling of f_{closed} indicates that the presence of those polymers in films grown with large G is negligible. Moreover, the closed polymers have sizes much below the average for large G [the average size of all polymers increases with $G^{1/2}$, as will be shown below]. For this reason, the statistics including and not including closed polymers give similar results. In the following we only present averages among all polymers.

Although the results in Figs. 2(a), 2(b), and 3(c) suggest that the polymers are stretched in the vertical direction, here we confirm it quantitatively by measuring typical polymer lengths in the two spacial directions. We calculated the rms fluctuations of the horizontal (x) and vertical (z) positions of

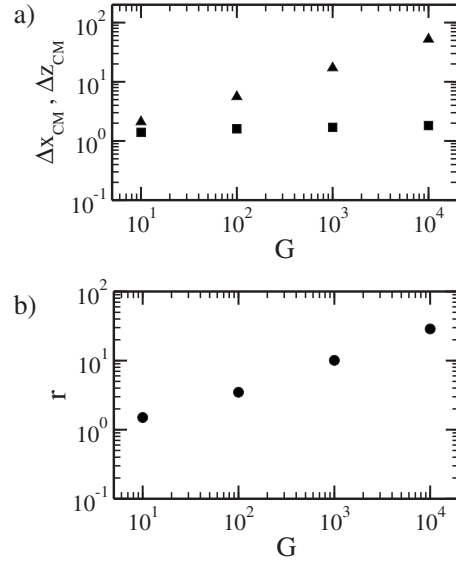


FIG. 7. (a) rms fluctuation of monomer positions in the horizontal (x , squares) and vertical (z , triangles) directions as a function of G . (b) Aspect ratio as a function of G . Data are from lattice size $L = 1024$.

the monomers relatively to the center of mass of the polymer, respectively called Δx_{CM} and Δz_{CM} . They are plotted in Fig. 7(a) as a function of G . In Fig. 7(b), we show the aspect ratio

$$r \equiv \Delta z_{CM} / \Delta x_{CM} \quad (11)$$

as a function of G .

As G varies three orders of magnitude, the change in Δx_{CM} is very small, while Δz_{CM} continuously increases. For $G \leq 10^2$ the polymers have aspect ratios of order 1, thus they are not significantly stretched yet. Indeed, one of the polymers highlighted in Fig. 2(a) is longer in the horizontal direction. Also note that the maximal polymer sizes shown in Fig. 3(c) for $G=10$ are in the SAW regime of slope $3/4$, which is not a regime of elongated polymers. On the other hand, the aspect ratio becomes large (r above 10) for $G \geq 10^3$, showing clear evidence of stretching in the vertical direction. This is consistent with the regime of slope 1 in the plots of Fig. 3(c) for large G .

The quantities most frequently used to characterize the polymer size are the average size $\langle S \rangle$ and the average end-to-end distance $\langle R_{ee}^2 \rangle^{1/2}$. Figure 8(a) shows these two quantities as a function of G . They are expected to scale with the same exponent as the rms z size because they represent typical lengths of the same set of polymers,

$$\langle S \rangle, \langle R_{ee}^2 \rangle^{1/2}, \Delta z_{CM} \sim G^\nu. \quad (12)$$

Since correction terms are possible in Eq. (12) (for any of those quantities), we calculated the effective exponents

$$\nu(G) \equiv \frac{\ln[\langle S \rangle(G) / \langle S \rangle(G/10)]}{\ln 10}, \quad (13)$$

for $\langle S \rangle$, and corresponding effective exponents for $\langle R_{ee}^2 \rangle^{1/2}$ and Δz_{CM} . Figure 8(b) shows those exponents as a function of $1/G^{1/2}$. An asymptotic value $\nu \approx 1/2$ (in the limit $G \rightarrow \infty$)

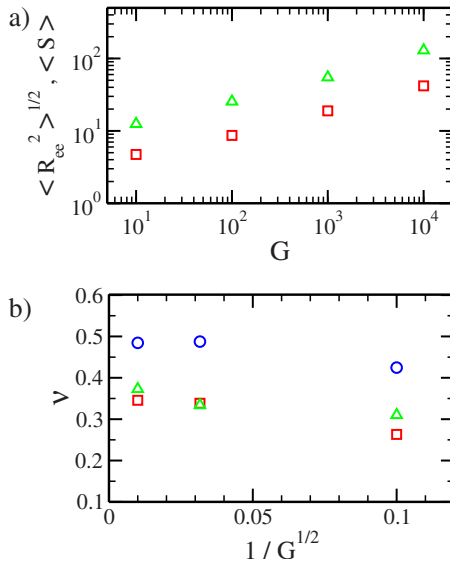


FIG. 8. (Color online) (a) Average polymer size (triangles) and rms end-to-end distance (squares) as a function of G . (b) Effective exponent $\nu(G)$ as a function of $1/G^{1/2}$ for the same quantities of (a) and for the rms fluctuation of monomer positions in the z direction (circles). Data are from lattice size $L=1024$.

is obtained for the rms z size. However, the effective exponents for the other quantities seem to converge to slightly smaller values, between 0.35 and 0.4, which indicates a slower growth in this range of G .

This discrepancy is certainly related to corrections to scaling in some of those quantities and makes it difficult to interpret the microscopic system dynamics based only on numerical data. However, we can explain the asymptotic value $\nu=1/2$ by properties of trapping of one-dimensional random walkers, as follows.

Since the polymers have large spaces separating them, particularly for large G , most monomers that collide with a polymer are confined to move along that chain, and most steps are in the vertical direction. After G steps, the incident monomer may find a polymer end or may stop moving and nucleate a new chain. The first process (chain propagation) is equivalent to the problem of trapping of a random walker by static traps at the end of a finite segment. The size of this segment is the typical polymer size, hereafter referred as S . In the one-dimensional trapping problem in a segment of size S , the probability of survival of the random walker after t steps is [46,47]

$$P_{surv} = 8/\pi^2 \exp(-\pi^2 t/S^2). \quad (14)$$

For a small polymer (small S) and large G , after $t=G$ steps we have very small P_{surv} , thus that polymer will grow. The polymer stops growing only when P_{surv} is of order 1 after executing $t=G$ steps; in this case, the nucleation of a new polymer is significantly probable. This occurs when $G/S^2 \sim 1$, which gives $\nu=1/2$ in Eq. (12). An interesting point of this reasoning is that a bulk property was obtained through the analysis of processes taking place near the outer surface of the deposit, similarly to other recent works [22,25].

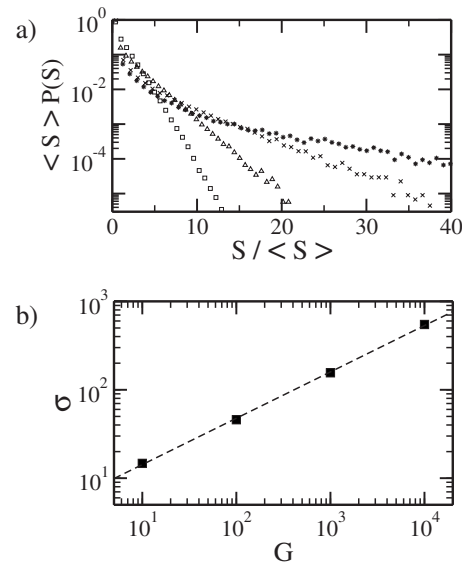


FIG. 9. (a) Scaled distributions of polymer sizes, where $P(S)$ is the probability of finding a polymer of size S . The symbols correspond to the same values of G of Fig. 4. (b) Scaling of the rms fluctuation of polymer size. The dashed line is a linear fit of the data. Data are from lattice size $L=1024$.

We conclude that the small values of exponents in Fig. 8(b) for $\langle S \rangle$ and $\langle R_{ee}^2 \rangle^{1/2}$ are a consequence of huge corrections to the dominant scaling of Eq. (12) since they do not show evidence of converging to $\nu=1/2$ as $1/G^{1/2} \rightarrow 0$. Certainly a much faster growth of those quantities is expected for $G > 10^4$.

Polymer relaxation and finite reaction rates may change these results, but it is difficult to anticipate a general trend. Large G corresponds to low monomer fluxes or high temperatures, where the polymers have longer times to relax to more compact configurations. The lower film densities after deposition also increase the free space for relaxation. This reduces the tendency to stretch. On the other hand, there is experimental evidence that the increase in chain mobility (via introduction of a solvent species) helps the formation of longer polymers because it facilitates the capture of diffusing monomers [6], and the larger polymers tend to stretch due to the confinement. There are also nontrivial cases, like that of poly(isobenzofuran) films [13], where a nonmonotonic variation of polymer size with substrate temperature is found.

Finally, we analyze the distribution of polymer sizes, whose scaled forms are shown in Fig. 9(a) for all values of G . $P(S)dS$ is defined as the probability of finding a polymer of size between S and $S+dS$ in a deposit. In all cases, the distributions are monotonically decreasing, thus there is a large fraction of small polymers in the films. For $G=10$, a fit $P(S) \approx 1/\langle S \rangle \exp(-S/\langle S \rangle)$ is good. For larger G , there is a depletion in the fraction of polymers with sizes below $2\langle S \rangle$ ($G=10^2$) to $5\langle S \rangle$ ($G=10^3$), and the right tail of the distributions has large weight. This means that there is a high probability of finding polymers much larger than the average in a sample. The general form of the right tails is $P(S) \sim \exp(-S/S_c)$, where S_c is a characteristic length that increases faster than $\langle S \rangle$ for $10 \leq G \leq 10^4$.

Another useful quantity to characterize those distributions is the rms fluctuation σ in the polymer size, which is plotted

in Fig. 9(b) as a function of G . The linear fit gives $\sigma \sim G^{1/2}$ without significant corrections, which is an apparently faster increase than that of $\langle S \rangle$ [see effective exponents for $\langle S \rangle$ in Fig. 8(b)]. However, it is important to stress that the asymptotic scaling of S_c and $\langle S \rangle$ is certainly the same because both quantities characterize the typical polymer size, thus that result is valid only in a finite range of G .

The size distribution of our model may be broad compared to peaked (monomodal) ones, but much broader ones are found in models of irreversible and reversible polymer brushes of Refs. [48,49], where power-law distributions were obtained. In those cases, polymer growth occurs by diffusion-limited aggregation of monomers in a solution, which favors growth of protuberant tips of the longer polymers. Knowing the shape of the polymer size distribution is very important for applications. For instance, a growth process with the same scaling of our model is not interesting for applications which require a narrow size distribution of the chains, but may be interesting if some mechanical property is related to a minimum fraction of polymers above a given size.

VI. CONCLUSION

We discussed a model for chemical vapor deposition polymerization accounting for the diffusion of monomers after their attachment to the deposit. Comparison with a previous full diffusion model [19] for that process shows many similar features, such as the increase of surface roughness and decrease of density with increasing monomer mobility. We analyzed the relation between characteristic polymer sizes and

the ratio $G \equiv D/F$ between monomer diffusion coefficients and external flux, and showed that the problem of random walk trapping explains those relations. The distributions of polymer sizes are typically broad, thus polymers much larger than the average values are highly probable in a sample. The surface roughness follows KPZ scaling, but exponent estimates show huge finite-size corrections. This result, obtained in a model with collimated monomer flux, is quite different from the ones obtained in previous CDVP models with oblique monomer fluxes and dimer nucleation [19,20], which show anomalous scaling.

The main results of our work are concerned with surface roughness scaling (on length and time), polymer size scaling (on diffusion to deposition ratio) and polymer size distribution. Despite the model being relatively simple and being simulated in two dimensions, the arguments used to explain those results are general. They are of qualitative nature, but focus on universal features and highlight the relevance of different physicochemical processes, including the type of monomer flux toward the surface. Thus, they certainly can be extended to three-dimensional deposits and more complex polymer dynamics. For this reason, we believe that our results are a helpful starting point for modeling real CVDP. The numerical framework presented here may be useful for the analysis of data of experiments and more complex models.

ACKNOWLEDGMENTS

J.A.R.E. acknowledges support from CNPq and FAPAR acknowledges support from CNPq and FAPERJ (Brazilian agencies).

-
- [1] W. A. Tenhaeff and K. K. Gleason, *Adv. Funct. Mater.* **18**, 979 (2008).
- [2] K. Kim, M. Y. Jung, G. L. Zhong, J.-I. Jin, T. Y. Kim, and D. J. Ahn, *Synth. Met.* **144**, 7 (2004).
- [3] S. Pursel, M. W. Horn, M. C. Demirel, and A. Lakhtakia, *Polymer Commun.* **46**, 9544 (2005).
- [4] H.-Y. Chen, Y. Elkasabi, and J. Lahann, *J. Am. Chem. Soc.* **128**, 374 (2006).
- [5] H.-G. Choi, J. P. Amara, T. P. Martin, K. K. Gleason, T. M. Swager, and K. F. Jensen, *Chem. Mater.* **18**, 6339 (2006).
- [6] X. Chen and M. Anthamatten, *Polymer Commun.* **49**, 1823 (2008).
- [7] M. C. Demirel, *Colloids Surf., A* **321**, 121 (2008).
- [8] Y. Elkasabi and J. Lahann, *Macromol. Rapid Commun.* **30**, 57 (2009).
- [9] Y.-P. Zhao, J. B. Fortin, G. Bonvallet, G.-C. Wang, and T.-M. Lu, *Phys. Rev. Lett.* **85**, 3229 (2000).
- [10] A. I. Buzin, D. S. Bartolome, K. A. Mailyan, A. V. Pebalk, and S. N. Chvalun, *Polym. Sci., Ser. A Ser. B* **48**, 961 (2006).
- [11] J. Zhou and C. A. Wolden, *Thin Solid Films* **430**, 28 (2003).
- [12] I. J. Lee, M. Yun, S.-M. Lee, and J.-Y. Kim, *Phys. Rev. B* **78**, 115427 (2008).
- [13] H.-G. Choi, J. P. Amara, T. M. Swager, and K. F. Jensen, *Macromolecules* **39**, 4400 (2006).
- [14] J. Lahann, D. Klee, and H. Hocker, *Macromol. Rapid Commun.* **19**, 441 (1998).
- [15] J. Lahann and R. Langer, *Macromolecules* **35**, 4380 (2002).
- [16] J. B. Fortin and T.-M. Lu, *Chem. Mater.* **14**, 1945 (2002).
- [17] K. K. S. Lau and K. K. Gleason, *Macromolecules* **39**, 3695 (2006).
- [18] Y.-P. Zhao, A. R. Hopper, G.-C. Wang, and T.-M. Lu, *Phys. Rev. E* **60**, 4310 (1999).
- [19] W. Bowie and Y.-P. Zhao, *Surf. Sci.* **563**, L245 (2004).
- [20] S.-W. Son, M. Ha, and H. Jeong, *J. Stat. Mech.* (2009) P02031.
- [21] J. W. Evans, P. A. Thiel, and M. C. Bartelt, *Surf. Sci. Rep.* **61**, 1 (2006).
- [22] E. Katzav, S. F. Edwards, and M. Schwartz, *Europhys. Lett.* **75**, 29 (2006).
- [23] F. A. Silveira and F. D. A. Aarão Reis, *Phys. Rev. E* **75**, 061608 (2007).
- [24] M. Kardar, G. Parisi, and Y.-C. Zhang, *Phys. Rev. Lett.* **56**, 889 (1986).
- [25] S. Tarafdar and S. Roy, *Physica B* **254**, 28 (1998); R. Karmakar, T. Dutta, N. Lebovka, and S. Tarafdar, *Physica A* **348**, 236 (2005).
- [26] T. J. Oliveira and F. D. A. Aarão Reis, *J. Appl. Phys.* **101**, 063507 (2007); *Phys. Rev. E* **76**, 061601 (2007).
- [27] S. Das Sarma and P. Tamborenea, *Phys. Rev. Lett.* **66**, 325

- (1991).
- [28] D. Wolf and J. Villain, *Europhys. Lett.* **13**, 389 (1990).
- [29] F. Biscarini, P. Samori, O. Greco, and R. Zamboni, *Phys. Rev. Lett.* **78**, 2389 (1997).
- [30] D. Tsamouras, G. Palasantzas, and J. Th. M. de Hosson, *Appl. Phys. Lett.* **79** 1801 (2001); *Surf. Sci.* **507–510**, 357 (2002); D. Tsamouras and G. Palasantzas, *Appl. Phys. Lett.* **80**, 4528 (2002).
- [31] D. Rodríguez-Pérez, J. L. Castillo, and J. C. Antoranz, *Phys. Rev. E* **76**, 011407 (2007).
- [32] B. Nienhuis, *Phys. Rev. Lett.* **49**, 1062 (1982); A. J. Guttmann, *J. Phys. A* **20**, 1839 (1987); A. J. Guttmann and J. Wang, *ibid.* **24**, 3107 (1991).
- [33] M. J. Vold, *J. Colloid Sci.* **14**, 168 (1959); *J. Phys. Chem.* **63**, 1608 (1959).
- [34] A. L. Barabási and H. E. Stanley, *Fractal Concepts in Surface Growth* (Cambridge University Press, Cambridge, England, 1995).
- [35] W. E. Hagston and H. Ketterl, *Phys. Rev. E* **59**, 2699 (1999).
- [36] F. L. Forgerini and W. Figueiredo, *Phys. Rev. E* **79**, 041602 (2009).
- [37] F. D. A. Aarão Reis, *Phys. Rev. E* **63**, 056116 (2001).
- [38] R. Miranda, M. Ramos, and A. Cadilhe, *Comput. Mater. Sci.* **27**, 224 (2003).
- [39] E. Katzav and M. Schwartz, *Phys. Rev. E* **70**, 061608 (2004).
- [40] A. Chame and F. D. A. Aarão Reis, *Surf. Sci.* **553**, 145 (2004).
- [41] J. M. López, *Phys. Rev. Lett.* **83**, 4594 (1999).
- [42] S. F. Edwards and D. R. Wilkinson, *Proc. R. Soc. London* **381**, 17 (1982).
- [43] F. D. A. Aarão Reis, *Physica A* **316**, 250 (2002).
- [44] G. Foltin, K. Oerding, Z. Rácz, R. L. Workman, and R. K. P. Zia, *Phys. Rev. E* **50**, R639 (1994).
- [45] T. Antal, M. Droz, G. Györgyi, and Z. Rácz, *Phys. Rev. E* **65**, 046140 (2002).
- [46] N. D. Donsker and S. R. S. Varadhan, *Commun. Pure Appl. Math.* **32**, 721 (1979).
- [47] D. ben-Avraham and S. Havlin, *Diffusion and Reactions in Fractals and Disordered Systems* (Cambridge University Press, Cambridge, England, 2000).
- [48] J. P. Wittmer, M. E. Cates, A. Johner, and M. S. Turner, *Europhys. Lett.* **33**, 397 (1996).
- [49] A. Milchev, J. P. Wittmer, and D. P. Landau, *J. Chem. Phys.* **112**, 1606 (2000).